arXiv:astro-ph/0001043v1 4 Jan 2000

Photometric Properties of 47 Clusters of Galaxies: I. The Butcher-Oemler Effect

V. E. Margoniner [1,2] and R. R. de Carvalho [2]
Email: vem@physics.bell-labs.com, reinaldo@on.br

ABSTRACT

We present *gri* CCD photometry of 44 Abell clusters and 4 cluster candidates. Twenty one clusters in our sample have spectroscopic redshifts. Fitting a relation between mean g, r and i magnitudes, and redshift for this subsample, we have calculated photometric redshifts for the remainder with an estimated accuracy of ~ 0.03. The resulting redshift range for the sample is $0.03 < z < 0.38$. Color-magnitude diagrams are presented for the complete sample and used to study evolution of the galaxy population in the cluster environment. Our observations show a strong Butcher-Oemler effect (Butcher & Oemler 1978, 1984), with an increase in the fraction of blue galaxies (f_B) with redshift that seems more consistent with the steeper relation estimated by Rakos and Schombert (1995) than with the original one by Butcher & Oemler (1984). However, in the redshift range between ~ 0.08 and 0.2, where most of our clusters lie, there is a wide range of f_B values, consistent with no redshift evolution of the cluster galaxy population. A large range of f_B values is also seen between ~ 0.2 and 0.3, when Smail at al. (1998) x-ray clusters are added to our sample. The discrepancies between samples underscore the need for an unbiased sample to understand how much of the Butcher-Oemler effect is due to evolution, and how much to selection effects. We also tested the idea proposed by Garilli et al. (1996) that there is a population of unusually red galaxies which could be associated either with the field or clusters, but we find that these objects are all near the limiting magnitude of the images ($20.5 < r < 22$) and have colors that are consistent with those expected for stars or field galaxies at $z \sim 0.7$.

Subject headings: galaxies: clusters – evolution – color – photometry

[1]Bell Laboratories, Lucent Technologies, Murray Hill, NJ 07974

[2]Observatório Nacional, CEP 20921-400, Rio de Janeiro, Brazil

1. INTRODUCTION

The existence of a linear locus in the color-magnitude diagram is a main characteristic of the early-type galaxy population in clusters. The effect in which the brightest galaxies are also the most red ones was studied in a systematic way by various authors. Visvanathan & Sandage (1977) obtained spectral energy distributions (SEDs) over a wide range of wavelengths for Virgo cluster galaxies and were one of the first to establish not only the existence, but also the dependence of the slope of the color-magnitude relation with wavelength.

The slope of the color-magnitude relation can be explained as an age effect, implying that the most luminous, massive galaxies, are older, or as a metallicity effect, consistent with the most luminous galaxies being more metal rich. *Hubble Space Telescope* (HST) observations have shown that the color-magnitude relation continues to be very well defined for early-type galaxies in high redshift clusters up to $z \sim 1$ (Standford et al. 1998, Kodama et al. 1998, Ellis et al. 1997), as well as in the field (Kodama et al. 1999). These observations suggest that at high redshift the early-type population already consists of old, passively evolving systems. Ellis et al. (1997), Standford et al. (1998) estimated that these galaxies were formed at $z > 2$, and therefore the color-magnitude relation can not be explained as a purely age effect. Also, Terlevich et al. (1999) used spectral absorption line indices, together with broad band photometry, to investigate how mean age and metal abundance correlate with galaxy luminosity and find that the color-magnitude relation in Coma is driven primarily by a luminosity-metallicity correlation.

However, recent observations by Worthey (1996) indicate that star formation is still occurring in $\sim 2/3$ of low redshift ellipticals and that many of these galaxies have ages less than half a Hubble time. The scatter in age of the early-type galaxy population can still be consistent with a well defined color-magnitude relation if galaxies assembling more recently are on average more metal-rich than older galaxies of same luminosity (Ferreras et al. 1998), which is consistent with Worthey's observations that show a trend for younger large galaxies to be more metal rich.

The luminosity-metallicity relation can be created as a result of the different efficiency of supernova galactic winds to eject gas from galaxies with different masses (Larson 1974). Massive galaxies are able to retain a high fraction of their gas, becoming more enriched than less massive galaxies which tend to lose their gas more easily. Another possible explanation for the origin of the luminosity-metallicity relation is the difference in merging dynamics between systems of different luminosities (Bekki and Shioya 1997). If the more luminous elliptical galaxies are formed by galaxy merging with more rapid star formation, less gas is tidally stripped from these systems during merging, and as a result a greater amount of the gas is enriched.

The universality of the color-magnitude relation (Visvanathan & Sandage 1977, Bower et al. 1992) makes it a powerful tool to study characteristics of the cluster galaxy population and its evolution. Butcher and Oemler (1978) observed the central regions of two rich, high redshift clusters of galaxies (CL 3C 295 at z=0.46 and CL 0024+1654 at z=0.39) and found an excess of blue galaxies in comparison to the typical early-type population which is found in the central

region of local clusters (Dressler 1980). In 1984, Butcher & Oemler published a study of 33 clusters in the redshift range between z=0.003 and 0.54 and confirmed that the fraction of blue galaxies in the inner region of clusters, where 30% of their galaxy population is found, increases with redshift. Butcher and Oemler's results were interpreted as detection of evolution in the population of galaxies, and many works regarding the nature of the blue galaxies followed.

Larson et al. (1980) suggested an evolutionary connection between S0 and spiral galaxies as the physical origin of the enhanced star formation in moderate redshift galaxies. The authors argue that S0s might be disk systems that lost their gas envelopes during the cluster collapse and consumed their remaining gas by star formation. This idea can explain the population of blue galaxies observed by Butcher and Oemler as spiral galaxies seen just before running out of gas, and the disappearance of this population in more evolved, low redshift rich clusters (Dressler et al. 1997, Couch et al. 1998). This idea is also in agreement with observations showing that the blue population lies preferentially in the outer edges of the cluster (Butcher and Oemler 1984, Rakos et al. 1997). Also, early-type galaxies in dense clusters are less metal-enriched than their counterparts in lower density environments (Rose et al. 1994), suggesting the truncation of star-formation in high density regions. The idea that the Butcher-Oemler effect is an evolutionary phenomenon is also reinforced by observations showing that star formation similar to that seen in distant clusters is still ongoing, although at a reduced level, in local clusters (Caldwell and Rose 1997).

HST images allowed the determination of the morphology of galaxies in high redshift clusters (Dressler et al. 1994, Couch et al. 1994, 1998). These data suggest that the blue Butcher-Oemler galaxies are predominantly normal late-type (i.e. small B/D ratios) spirals but also that dynamical interactions and mergers between galaxies may be an important process responsible for the star formation enhancement in those galaxies. Oemler et al. (1997) presented HST obsevations of four rich clusters at $z \sim 0.4$ confirming that most of the blue Butcher-Oemler galaxies have colors, luminosities and spatial distributions similar to the normal galaxies observed at low redshift. The authors show however that $\sim 30\%$ of these "normal" galaxies show abnormal patterns of star formation such as rings. Oemler et al. (1997) also find a large fraction of m/i galaxies, but argue that these objects can not account for most of the blue Buther-Oemler galaxies. m/i galaxies do not follow the spatial distribution of the the blue Buther-Oemler objects, instead they are concentrated at the dense regions of the cluster following the distribution observed for E/S0 galaxies. Furthermore, Oemler et al. (1997) show that the m/i galaxies are too few to account for the Buther-Oemler galaxies. Rakos et al. (1996) used narrowband photometry to study Butcher-Oemler galaxies and also found that the blue population consists of spiral-like systems with the addition of a small fraction of bright, blue interacting and merger systems. Rakos and Schombert (1995) find that the fraction of blue galaxies increases from 20% at $z = 0.4$ to 80% at $z = 0.9$, suggesting that the evolution in clusters is even stronger than previously indicated by Butcher and Oemler.

Although the Butcher-Oemler effect has been debated in many studies, and many evolutionary

theories have been proposed, there are some suggestions of strong selection biases in Butcher and Oemler's original sample of clusters. Newberry et al. (1988) measured velocity dispersions and surface density of galaxies in clusters and found that there is a marked difference between local clusters and intermediate redshift ones. More recently, Andreon and Ettori (1999) measured x-ray surface brightness profiles, size, and luminosity of the Butcher-Oemler sample of clusters and conclude that this sample is not formed from the same kind of objects observed over a range of look-back times. The selection effects are not well understood, and might be mimicking evolutionary effects. Smail et al. (1998) used a well defined sample of 10 clusters in the redshift range $z = 0.22 - 0.28$ with high x-ray luminosity, and found that these massive clusters contain only a small fraction of blue galaxies. The Butcher-Oemler effect is not observed in this sample.

Also, in a visually selected sample of clusters, the presence of false structures, identified as clusters due to projection effects, is expected. The color of the galaxy population at such regions will tend to be bluer than observed in clusters, and the inclusion of these false clusters in the study of the Butcher-Oemler effect will tend to increase the number of structures with high fraction of blue galaxies. It is therefore important to be very careful in interpreting results from samples which might be biased, and the need for a well defined, statistically significant sample of clusters to study evolutionary effects is evident.

Garilli et al. (1995, 1996) observed clusters in the redshift range $0.05 \leq z \leq 0.25$ and used the color-magnitude relation to study their galaxy populations. The authors estimated the fraction of blue galaxies and did not find signs of evolution, but noticed the presence of a rather large number of red galaxies, with both $g-r$ and $r-i$ colors at least 0.3^m redder than the early-type sequence in the color-magnitude diagrams. These objects accounted for $\sim 7\%$ of the total galaxy population. They also noticed that about 1/3 of these red galaxies had $19.5 < m_r < 22$ and $r - i > 1$ which are typical of field galaxies at $z > 0.7$, but their $g - r \sim 1.2$ colors were not red enough for these galaxies to be at such a high redshift. The existence of such a population of galaxies would be very important for the models of stellar population in elliptical galaxies, and for this reason we used the same methodology as Garilli et al. (1996) to search for a red galaxy population in our sample.

The slope, intercept, and scatter of the color-magnitude relation can also be used to study the evolution of galaxy population in clusters. Many authors (Rakos and Schombert 1995, Ellis et al. 1997, Gladders et al. 1998, Kodama et al.1998, Standford et al. 1998, Pahre 1998, 1999) have found that the observations are consistent with models in which most early-type galaxies in rich clusters are old, passively evolving systems. Bower et al. (1998) proposed a model on which star formation occurs over an extended period of time in most galaxies with star formation being truncated randomly. This type of star formation allows both for the small scatter of the color-magnitude relation which is observed up to $z \sim 1$, and for the presence of the blue galaxy population at intermediate redshift clusters (Butcher-Oemler effect).

Bower et al. (1998) have also shown how is it possible to use the color-magnitude relation as a constraint on the formation of rich clusters. Mergers will tend to reduce the slope and increase the

scatter of the color-magnitude relation, therefore, the ratio between the scatter and the slope of the relation can be used to study the degree of merging between pre-existing stellar systems. The authors analyze the cases of random and hierarchical mergers and show that the first case would tend to very rapidly destroy the relation and that the second case allows for the color-magnitude relation to persist through a larger number of mergers.

In this work we present the color-magnitude relation for 48 clusters, and then use them to study the Butcher-Oemler effect, and to search for a population of red galaxies in the sample. In order to study the Butcher-Oemler effect, we need to know the redshifts of the clusters. We use the 21 clusters for which there are spectroscopic redshift measurements to construct an empirical relation that allows the estimation of photometric redshifts for the remainder. The paper is organized as follows. In §2 we describe the observations and data reduction. §3 gives a description of the galaxy catalog construction. The results are presented in §4, and the summary and conclusions are shown in §5. We will examine the evolution of the color-magnitude relation and investigate the merger history of the galaxy population in a forthcoming paper.

2. OBSERVATIONS AND DATA REDUCTION

2.1. Observations

We obtained CCD images of 48 clusters in four runs between March 1997 and November 1998. All data were taken with the Tek 2K-3 detector at the Cassegrain focus of the 0.9m telescope at the Cerro Tololo Interamerican Observatory (CTIO). The CCD has 2048 x 2048 pixels, each pixel covering $0.396''$, corresponding to a field of $\sim 13.5'$ x $13.5'$, or $\sim 0.5 - 6.7$ Mpc at $z = 0.03 - 0.38$ ($H_0 = 67$ Km s^{-1} Mpc^{-1}). We observed 44 Abell clusters and 4 cluster candidates detected in POSS-II (Second Palomar Sky Survey) (Gal et al. 1999) photographic plates. The images were taken through the g, r and i filters of the Thuan & Gunn (1976) photometric system, with effective wavelengths and widths of 5118 Å and 900 Å for g, 6798 Å and 1000 Å for r, and 8100 Å and 1500 Å for i. The exposure times varied between 15-60 minutes in the g band, 10-20 minutes in the r band, and 10-15 minutes in the i band.

Details of the observations are shown in Table 1. In column 1 the ACO (Abell, Corwin & Olowin 1989) cluster number or the candidate identification is given; column 2 shows the observation date; columns 3, 4 and 5 list the exposure times in the g, r and i bands; the seeing is given in columns 6, 7 and 8, and the limiting magnitudes (see section 3.2) are listed in columns 9, 10 and 11 for each band.

2.2. Data Reduction

The raw images were corrected for the usual instrumental effects of *"bias"*, *"dome flat"*, *"sky flat"*, and *"illumination"*. It was also necessary to apply a *"shutter"* correction for short exposure images ($T_{exp} < 20sec$) such as *"dome flats"* and standard stars. In this case, the time for the shutter to open and to close is important compared to the total exposure time and therefore the borders of the CCD collect photons for a shorter time than its central part.

2.3. Photometric Calibration

The photometric calibration of the magnitude scale was determined by the observation of ~ 5 standard stars from the Thuan & Gunn (1976) list in each night. The color equation, which establishes the relation between instrumental and calibrated magnitudes, is given by eq.(1).

$$g_{cal} = g_{inst} + A + B\mathrm{sec}(z) + C(g-r)_{inst} \quad (1)$$

where A is the zero point of the magnitude scale; B is the extinction coefficient; and C is the color term coefficient. Similar color equations were determined for the r and i bands, with the color terms established from the $g-r$ and $g-i$ colors respectively.

When possible, the color equations were determined for each night in the three photometric bands. Because the number of standard stars with i calibration is very limited, there were nights when we did not observe enough standard stars in this band to allow us to determine this calibration. However, we found that the color equation coefficients were always in close agreement for the nights within a specific run. We therefore used the stars observed in each run to derive mean g, r and i color equations (i.e. A, B and C coefficients) for each run. The color equations derived for each run showed rms errors of at most 0.025^m in g, 0.017^m in r, and 0.009^m in i. These errors could justify the use of the same color equations for each entire run, but in order to avoid small systematic errors we decided to use the zero points of the magnitude scale estimated individually for each night. The zero points determined using the mean extinction and color term coefficients previously calculated for each run are listed in Table 2, and have errors that are consistent with the rms values of the color equations. In Figure 1 we show the comparison between magnitudes of standard stars published by Thuan & Gunn (1976) and our final calibrated measurements.

2.3.1. External Errors

The external photometric errors were estimated by comparison between the measurements of clusters that were observed in different nights and runs. Abell cluster 2700 was observed in three different nights, and two other clusters (A248, and A324) were observed twice. Figure 2 shows the

residuals of the magnitudes, in each band, for Abell 2700. The residuals are calculated from the galaxies brighter than the limiting magnitude (see §3.2) of the CCD images, and we found mean values of 0.042 in g, 0.017 in r, and 0.048 in i, which are of the same order as the rms values of the color equation.

3. GALAXY CATALOG CONSTRUCTION

3.1. Detection and Classification

The detection and classification of objects in the CCD images were performed using a modified version of the FOCAS (Faint Object Classification and Analysis System, Valdes 1982) package. The first step in the construction of those catalogs is the detection of objects. We used a detection limit of two times the standard deviation of the background sky, which corresponds to $\sim$7% of the local sky value. We used also a minimal detection area of 25 pixels, which is ~ 2 times greater than the average seeing disc.

FOCAS calculates about 30 photometric attributes for each detected object, including the total and aperture magnitudes. The total magnitude is determined with the use of an algorithm which extends the detection isophote to lower surface brightness limits. When the area of the extended isophote become two times bigger than the area of the initial detection isophote the total magnitude is computed. The aperture magnitude is calculated from the flux inside a central circular region of radius $5.15''$.

Another important step in the construction of the CCD catalogs is the determination of the point spread function (PSF) which is used in the classification procedure. Stellar, non-saturated, objects with magnitudes between 16^m and 19^m are selected to construct the PSF. A visual inspection on the objects selected by FOCAS as stars allowed us to exclude asymmetric objects, and the final PSF for each image was determined with typically 35 stars. The classification of the objects was performed by FOCAS using the determined PSF (Valdes 1982). To avoid the inclusion of clearly misclassified objects we carried out a visual inspection before the construction of the catalog (the data are available upon request).

3.2. Limiting Magnitude

The histogram of total magnitudes of all the detected objects (stars and galaxies) was used to estimate the limiting magnitude for each CCD image. This limiting magnitude was determined by the last bin of magnitude before the counts start to drop significantly (Picard 1991). The values are listed in Table 1 for each cluster, in the three photometric bands.

4. RESULTS

4.1. Color-Magnitude Diagrams

In Figure 3 we present the $r - i \times r$ and $g - r \times r$ color-magnitude relations for all the clusters in our sample. The linear fit shown by a solid line was, in general, determined using the galaxies in the magnitude range between $M^* - 1$ and $M^* + 2$, where $M^* = -20.91$ ($h = 0.75$) (Lin et al. 1996). Objects with $r < 16.0$ can be saturated in our images and were excluded from our analysis, and for this reason the limiting magnitude to fit the color-magnitude relation of the lower redshift clusters was extended to $M^* + 3$ (Abell 119, 168, 509, 1134, 2103) and $M^* + 4$ (Abell 189, 261, 1260, P861C1). Also, because the average limiting magnitude of our sample is $r \sim 22.0$, we excluded fainter objects from our fitting procedure. The data was binned in intervals of 0.5 mag, except for the first bin for which we impose that there should be at least 5 galaxies. We then used ROSTAT (Beers et al. 1990) to determine the median color and magnitude in each bin, as well as its bi-weight dispersion. The fitting procedure was done with the GaussFit program (Jefferys et al. 1988), which allows the usage of several methods for solving least squares and robust estimation problems. After testing many of these procedures, we decided to use the "Orthogonal Regression M-Estimates" (orm), considering the color dispersion in each magnitude bin, to fit the color-magnitude relation.

4.2. Photometric Redshifts

In order to study the Butcher and Oemler effect we need to know the redshift of the clusters. The 21 clusters with spectroscopic measured redshift were used in the construction of an empirical relation between redshift and mean gri magnitudes, that was then applied to estimate photometric redshifts for the remainder. The idea of estimating cluster redshifts using magnitudes and colors is based on the fact that in the central region of clusters the population is dominated by early-type galaxies (Dressler 1980, 1997). If we assume that the same SED is typical of all clusters, the apparent magnitude and consequentially the colors of these galaxies can be used to estimate redshifts because of the strong 4000 Åbreak feature typical of this population. We used the thirty brightest galaxies, after a statistical background correction, to estimate mean magnitudes representative of each cluster and fit a first order polynomial relation $z(g, r, i)$.

The background correction is very important if one is trying to study the cluster galaxy population, and it is also a difficult matter due to the field-to-field fluctuations on the number counts. Usually the best approach in estimating the back and foreground contamination is the use of an annulus around the cluster. Unfortunately the CCD images presented in this work sample only the central region of clusters and therefore it is not feasible to determine corrections for each cluster individually. We used the mean counts in 5 control fields to estimate the background magnitude distribution. The mean number of interlopers subtracted from each field is 12 with an

rms variation of ±4.6 among the 5 different control regions.

The comparison between spectroscopic and photometric redshifts is shown in Figure 4 and the dispersion of $z_{spect} - z_{phot}$ is $\sigma_z = 0.03$. This residual is of the same order as found by other works such as Connolly et al. (1995), Brunner et al. (1997), and Yee et al. (1999). Connolly et al. (1995) were the first to use an empirical approach to estimate photometric redshifts and using photographic data found a dispersion of $\sigma_z = 0.047$ when comparing spectroscopic and photometric redshifts for galaxies out to $z \sim 0.5$. Brunner et al. (1997), using CCD observations in 4 photometric bands, were able to obtain a relation with dispersion of $\sigma_z = 0.023$ for clusters in the redshift range between 0.0 and 0.4. Recently, Yee et al. (1999) used the C-M relation to determine redshifts with a mean dispersion of $\sigma_z = 0.028$ for clusters at $0.1 < z < 0.7$.

We also estimated photometric redshifts using only the early-type population of the clusters. The selection of cluster early-type galaxies can be done with an efficiency better than 90%, based on two-color and morphological information (Pahre 1998, 1999). The dispersion between spectroscopic and photometric redshifts obtained from the early-type galaxies brighter then 21^m is $\sigma_z = 0.04$. Comparing this result with the previous one, it is clear that using all the galaxies in the central region of the clusters is consistent with using elliptical galaxies only. This is consistent with the central region of rich, regular clusters being populated mainly by early-type galaxies (morphology-density relation, Dressler 1980, 1997).

Cluster coordinates and redshifts are presented in Table 3. The ACO cluster number or candidate identification is given in column 1; R.A. and Dec. coordinates for 1950 are listed in columns 2 and 3; the Abell richness class is given in column 4; The redshift is given in column 5, and the reference for this redshift is listed in column 6. Column 7 gives the fraction of blue galaxies calculated as described in 4.3.

4.3. Butcher-Oemler Effect

Butcher & Oemler (1984) (hereafter BO84) searched for signs of evolution in the galaxy population of clusters studying a sample of 33 clusters of galaxies with redshifts between 0.003 (Virgo) and 0.54. The galaxies brighter than $M_V = -20$, inside the central region containing 30% of the cluster population (R_{30}) were selected, and those with rest-frame $B - V$ colors at least 0.2 mag bluer than the ridge of the early-type galaxies in the color-magnitude diagrams were classified as "blue". The authors defined the fraction of blue galaxies (f_B) as the ratio between the number of blue and total number of galaxies, and found that f_B is approximately constant until $z \sim 0.1$ and starts to increase linearly for higher redshift clusters.

Our CCD images are $\sim 13.5'$ x $13.5'$ and sample only the central part of the clusters. For this reason it was not possible to determine R_{30} for each cluster individually and we decided to adopt a fixed physical size of radius 0.7 Mpc, which corresponds to the mean R_{30} used by BO84. We then selected the galaxies inside this region which, after k(z) correction, were found to be in the

magnitude range between $M^* - 1$ and $M^* + 3$, where $M^* = -20.91$ (Lin et al. 1996) assuming $h = 0.75$. The galaxies with $g - r$ colors at least 0.2 mag bluer than the locus of the early-type galaxies in the color-magnitude diagrams (Figure 3) were identified as blue, because a change of 0.2 mag in the $B - V$ color of an elliptical galaxy corresponds to approximately the same change in its $g - r$ color (Jorgensen 1995).

The background correction is very important in this study, and it tends to decrease f_B since the field galaxies are in general bluer than the early-type population typically found in the central region of clusters (Dressler 1980). BO84 estimated background corrections in different ways for different clusters, but their main idea was to use the population of galaxies around the clusters. Our fields are too small to allow such corrections, and therefore we used 5 control fields observed during the first run to estimate the background correction. Since the number of background galaxies contaminating each cluster depends on its redshift, and the number of background galaxies which would be identified as blue depends also on each cluster C-M relation, the background correction was applied individually. Usually, the number of galaxies r between $M^* - 1$ and $M^* + 3$ (where $M^* = -20.91$ assuming $h = 0.75$, Lin et al. 1996) detected in a cluster image is 94, and the background counts are 38, with a variation of ± 8 galaxies among the 5 different control regions. The number of blue galaxies in on average 23, and there are usually 9 ± 2 background galaxies that would be selected as blue.

Several corrections need to be applied to guarantee that the same physical region, and the same interval in the luminosity function (LF) of the clusters, are being used to compute the fraction of blue galaxies. Clusters at low redshift suffer from two different problems: 1) our CCD fields are not big enough to observe a region of radius 0.7 Mpc; and 2) the brightest objects (around $M^* - 1$) are saturated. For clusters at higher redshifts, the fainter objects (around $M^* + 3$) are not detected. To estimate the effect of measuring f_B at different regions in the cluster we used 5 clusters in the redshift range $z = 0.16 - 0.18$ for which the angular sizes are small, and for which the entire magnitude interval from $M^* - 1$ to $M^* + 3$ can be observed. The mean fraction of blue galaxies computed at different radius is shown in Figure 5, and the errorbars are $rms/\sqrt{5}$. Fitting a linear relation to the points we find:

$$f_B = 0.103 \times (R/0.7) + 0.185 \qquad (\sigma_{f_B} = 0.093) \tag{2}$$

where R is the radius in Mpc.

The idea that the fraction of blue galaxies increases in the outer parts of the cluster is in agreement with previous results. This behavior was already noticed by BO84 in their original work, and Rakos et al. (1997) also observe this trend in the detailed study of Abell 2317. This is also consistent with the work by Dressler and Gunn (1992), Dressler et al. (1994) and Oemler et al. (1997), which shows that early-type galaxies cluster more strongly than those with signs of recent or ongoing star-formation.

To estimate the effect of losing objects off the bright or faint ends of the chosen magnitude range, we use the sample of clusters at moderate redshift ($0.085 < z < 0.175$), for which we are

able to observe the entire interval of $M^* - 1$ to $M^* + 3$ and therefore to calculate f_B at various limiting magnitudes. The sample was subdivided in two ($0.085 < z < 0.130$ and $0.130 < z < 0.175$) in order to check if clusters at different redshifts show a different distribution of luminosities of its blue galaxy population. Figure 6a shows the result of missing the cluster brightest objects (f_B versus Δ_{mag}, where $\Delta_{mag} = (M^* + 3) - (M^* - ?)$), and Figure 6b indicates the effect of losing the faintest ones (f_B versus Δ_{mag}, where $\Delta_{mag} = (M^* + ?) - (M^* - 1)$). Two main results can be draw from these figures: (1) the fraction of blue galaxies inside a fixed radius of 0.7 Mpc is larger for clusters at higher redshift (open circles) than for the lower redshift ones (open squares) (Buther-Oemler effect); (2) f_B increases as brighter objects are excluded from the sample (Fig 6a) and decreases if the faint objects are missing (Fig 6b), indicating that the blue galaxy population is faint. The results are the same for the two subsamples, and the slope of the f_B versus Δ_{mag} relations does not show significant change with redshift. We therefore use the entire sample of clusters (between $0.085 < z < 0.175$) to estimate the effect of measuring f_B at different intervals of magnitude. The following two equations indicate the linear fits for losses from the bright and faint ends, respectively, obtained from the total mean points (solid dots).

$$f_B = -0.034 \times \Delta_{mag} + 0.362 \qquad (\sigma_{f_B} = 0.064) \tag{3}$$

$$f_B = +0.055 \times \Delta_{mag} + 0.016 \qquad (\sigma_{f_B} = 0.050) \tag{4}$$

The point at $\Delta_{mag} = 2.0$ in Figure 6b, corresponding to the magnitude interval between $M^* - 1$ and $M^* + 1$, was excluded from the fitting procedure. This point was ignored because when the faint objects are excluded the number of cluster galaxies drops dramatically, significantly increasing the errors in f_B. This effect is not as important when the brightest objects are missing, since the number of faint objects is always much larger than the number of bright objects. Although BO84 were limited to much brighter objects, they find the same tendency observed in our sample. The blue galaxies are also the faintest ones. Rakos et al. (1997) found an opposite trend in A2317 ($z = 0.211$). The authors calculated f_B at four magnitude bins and found that f_B is highest in the brighter bin, drops in the two intermediate bins, and rises again in the fainter one. The fact that the blue galaxies in more evolved, low redshift clusters are faint, and that a greater number of bright blue galaxies is found in higher redshift or less evolved clusters seems to support the idea that BO galaxies are late-type, low surface brightness objects, which fade after a burst of star formation (RS95).

The CCD images presented here are deeper than the photographic plates used by BO84, therefore allowing us to include fainter galaxies in our f_B estimate. On the other hand, BO84 were able to measure the brightest cluster objects that are usually saturated in our images. As it can be seen from Figures 6a and 6b the differences in the magnitude interval used to determine f_B strongly affects its measurements. In order to compare our results with BO84 we need to "correct" our fraction of blue galaxies as if we had used the same limiting magnitudes. If we assume that the typical $g - r$ color of an elliptical galaxy at $z = 0$ is 0.44 (Small 1996), the $M_V = -20$ limiting magnitude used by BO84 corresponds approximately to $M_r = -20.19$ (Jorgensen et al. 1995). This is the same as limiting our sample at $M^* + 0.72$, which results in a reduction of 0.13 (Figure

6b) from our f_B values. BO84 give no limiting magnitude for brighter objects, so we apply no correction for this effect. However, we do not expect this to be a major problem since it can be seen from Figures 6a and 6b (and equations 3 and 4) that the effect of missing bright objects is weaker than that of missing faint objects. Comparing the two clusters that we have in common with BO84, we find that their f_B measurements are 0.13 (for Abell 1689) and 0.16 (for Abell 370) lower than ours, indicating that our correction of 0.13 is reasonable.

The final fractions of blue galaxies are shown in column 7 of Table 3 and in Figure 7a. The quoted f_B errors are $(N)^{1/2}$ of the number of galaxies after background correction. Abell 1993 shows as extremely high fraction of blue galaxies (0.606 ± 0.141) that can be due to a wrong redshift estimation and/or to the common problem of projection effects existent in catalogs of clusters constructed from visual inspection of images. This is a not very well studied cluster and the last reference is from Abell et al. (1989) and for this reason we decide not to include it in Figure 7 and in the following discussion. Figure 7b shows the mean f_B values for intervals of 0.04 in redshift for the clusters with spectroscopic redshifts (filled circles), and for the clusters with estimated photometric redshifts (open circles). Both photometric and spectroscopic redshift samples show the same behavior in the $f_B \times z$ plot. In Figure 7c we plot the mean f_B values for the clusters in our sample (filled circles), for BO84's clusters (open squares), and for 10 x-ray clusters observed by Smail et al. (1998) (crosses). The solid and dashed lines shown in figure 7 represent respectively the relation originally found by BO84, and the one estimated by Rakos and Schombert (1995, hereafter RS95) in their study of 17 clusters. The dotted line represent a linear fit to the binned mean points from our sample.

In order to check the adherence of the points to BO84, RS95 and to our estimated $f_B \times z$ relation we plot in Figure 7d the accumulated product $f_B \times \Delta z$ for our data and for the three relations. The data seems more consistent with our relation and also with RS95 relation which is very similar to ours except for an offset due to the negative fraction of blue galaxies that we find at lower redshifts. The data shows an stronger increase in the fraction of blue galaxies with redshift than estimated by B084. The dot-dash line indicates the behavior assuming no evolution, or a constant f_B of 0.09. This is a mean value estimated from the clusters with spectroscopic redshiftin our sample, and it is clear that f_B is not constant: there is an absence of blue galaxies at local clusters, and an excess of blue objects at higher redshifts.

Andreon and Ettori (1999) used x-ray measurements of BO84 sample to argue that these clusters are not part of the same class of objects, and that therefore the increase in the fraction of blue galaxies with redshift might be simply a selection effect. Smail et al. (1998) studied the Butcher-Oemler effect in clusters at $0.22 - 0.28$ with similar x-ray luminosity, which should result in a sample consisting of the same kind of objects, and did not find the evolutionary trend shown in BO84, RS95 and in our data. Their observations, binned in redshift, are indicated by two crosses in Figure 7c and lie well below previous observations. It is interesting to note that if we concentrate our attention only in the redshift range between 0.08 and 0.2 (see Figure 7a), where we observed 10 times more clusters than BO84 and where most of our sample lies, we find objects

with a wide range in f_B. These observations, as well as Smail et al. (1998) measurements, might be indicating that the Butcher-Oemler effect is at least partially due to selection effects that are still not well understood. A complete, statistically significant sample of clusters, representative of all kinds of clusters at a certain redshift, should be able to resolve this question. Unfortunately, such a complete sample is very hard to observe, and any sample will always be biased toward richer, more luminous systems, but a very large sample should contain most kinds of clusters at a given redshift. With this purpose we are now analyzing a sample of ~ 500 clusters that were observed in the same way described in this work. This large CCD sample of Abell clusters was primarily obtained to calibrate the POSS-II (Second Palomar Sky Survey) photographic plates and is now also being used to study the population of galaxies in clusters and its evolution.

4.4. Anomalously Red Galaxies?

In each cluster we selected as red all the galaxies with $g - r$ and $r - i$ colors 0.3^m above the lines in Figure 3, and brighter than $m_r = 22^m$. The upper panels in Figure 8 show the histograms of m_r, $g - r$, and $r - i$ of the red galaxies. The filled histograms represent objects with $r - i \geq 1$. As it can be seen from upper panel, most of those objects are faint having m_r between 20.5^m and 22^m and have $g - r$ colors varying from ~ 0.8 up to 2.4. Objects with $g - r \sim 1.8$ are red enough to be in agreement with the observation of a high redshift ($z \sim 0.7$) population of galaxies with $r - i \geq 1$. Such red colors are due to the heavy k-corrections for elliptical galaxies at $z > 0.4$ (see Figure 2 of Gal et al. 1999 for $(g - r) \times (r - i)$ tracks for diferent types of galaxies as a function of redshift). At $z \sim 0.4$ the 4000 Åbreak feature typical of elliptical galaxies enters the g band causing a dramatic drop in its blue luminosity. The objects with $g - r \sim 1.2$ seem to correspond to the anomalously red galaxies found by Garilli.

Most of the stars with $r - i \geq 1$ have $g - r \sim 1.2$ (Kennefick 1996), so stellar contamination could be responsible for at least part of this red population. In order to study the seeing effect in this population, the sample was divided in two: one with better seeing ($FWHM < 1.44''$), and other with worse seeing ($FWHM > 1.44''$) in r band. The bad seeing observations shown in the central panels of Figure 8 present mainly one peak around 1.2^m on the $g - r$ distribution. But the $g - r$ distribution from the better seeing images (lower panels in Figure 8) shows also the presence of redder objects, which indicates that at least part of those anomalously red objects are in fact stars that were misclassified as galaxies. This effect should be even stronger for the Garilli et at. (1996) data, which had an average poor seeing of $2''$. Furthermore, only 42% of the "anomalously" red galaxies classified as galaxies in r were also classified as galaxies in g and i, while 71% of the rest of the r galaxies were classified as galaxies in all filters.

5. SUMMARY AND CONCLUSIONS

We present a photometric study of 48 clusters of galaxies. Color-magnitude diagrams are shown for the entire sample, and used to study the Butcher-Oemler effect and the population of red galaxies. We also present photometric redshifts for the clusters for which there are not spectroscopic measurements. The photometric redshift is estimated from the colors and magnitudes of cluster galaxies and has an accuracy of ~ 0.03. Our main conclusions are summarized as follows:

1. The blue, Butcher-Oemler galaxies, lie preferentially in the outer edges of the cluster, and are in general fainter than the cluster early-type population.

2. We find that the increase in the fraction of blue galaxies with redshift seems more consistent with the relation estimated by RS95 than with the original one by BO84. We predict a linear $f_B \times z$ relation consistent with RS95 estimation for $z > 0.08$ but in which the fraction of blue galaxies continues to decrease for lower redshifts. This result is consistent with the observation of a smaller number of blue galaxies in the cluster region than would be observed in a blank field region of the same angular area. However, there is no redshift evolution of f_B in the range between ~ 0.08 and 0.2, where most of our clusters lie. Also, a large range of f_B values is seen between ~ 0.2 and 0.3 when Smail et al. (1998) x-ray clusters are added to the $f_B \times z$ plot. We are currently analyzing a sample of ~ 500 clusters which might help in understanding the selection effects and may clarify the results.

3. Studying the population of red galaxies in our images we found that some of these objects have colors that are normal for background galaxies, and that the colors of the supposably anomalous red objects are typical of stars. The fact that these objects are near the limiting magnitude of our sample, and that they are found in greater number at the bad seeing images, lead us to the conclusion that at least part of those objects are stars that were misclassified as galaxies.

We would like to thank D. Wittman, J.A. Tyson, H.V. Capelato, R.R. Gal, and S.C. Odewhan for very helpful comments and suggestions which helped to improve the paper. We also thank the anonymous referee for the detailed revision and usefull recommendations provided for this work.

REFERENCES

Abell G.O., Corwin Jr.H.G., Olowin R.P., 1989, ApJS, 70, 1

Andreon S., Ettori S., 1999, ApJ, 516, 647

Beers T.C., Flynn K., Gebhardt K., 1990, AJ, 100, 32

Bekki K., Shioya Y., 1997, ApJ, 486, 197

Bower R.G., Kodama T., Terlevich A., 1998, MNRAS, 299, 1193

Bower R.G., Lucey J.R., Ellis R.S., 1992, MNRAS, 254, 601

Brunner R.J., Connolly A.J., Szalay A.S., 1997, ApJ, 482, 21

Butcher H., Oemler A.Jr., 1978, ApJ, 219, 18

Butcher H., Oemler A.Jr., 1984, ApJ, 285, 426 (BO84)

Caldwell N., Rose J.A., 1997, AJ, 113, 492

Connolly A.J., Csabi I., Szalay A.S., 1995, AJ, 110, 6

Couch W.J., Ellis R.S., Sharples R.M., Smail I., 1994, ApJ, 430, 121

Couch W.J., Barger A.J., Smail I., Ellis R.S., Sharples R.M., 1998, ApJ, 497, 188

Dixon K.L. Godwin J.G., Peach J.V., 1989, MNRAS, 239, 459

Dressler A., 1980, ApJ, 236, 351

Dressler A., Gunn J.E., 1992, ApJS, 78, 1

Dressler A., Oemler A.Jr., Butcher H.R., Gunn J.E., 1994, ApJ, 430, 107

Dressler A., Oemler A.Jr., Couch W.J., Smail I., Ellis R.S., Barger A., Butcher H.R., Poggianti B.M., Sharples R.M, 1997, ApJ, 490, 577

Ellis R.S., Smail I., Dressler A., Couch W.J., Oemler A.Jr., Butcher H.R., Sharples R.M, 1997, ApJ, 483, 582

Ferreras I., Charlot S., Silk J., 1998, ApJ, 521, 81

Fetisova T.S., Kuznetsov D.Y., Lipovetskii V.A., Starobinskii A.A.,Olovin R.P., 1993, AstL, 19, 198

Gal R.R., de Carvalho R.R., Odewhan S.C., Djorgovski S.G., Margoniner V.E., 1999, submitted to AJ, (astro-ph/9910173)

Garilli B., Bottini D., Maccagni D., Carrasco L., Recillas E., 1996, ApJS, 105, 191

Garilli B., Maccagni D., Carrasco L., Recillas E., 1995, *A.S.P Conf. Ser.*, 86, 297

Gladders M.D., López-Cruz O., Yee H.K.C., Kodama T., 1998, ApJ, 501, 571

Jefferys, W.H., Fitzpatric M.J., McArthur B.E., 1988 Celest. Mech., 41, 39

Jorgensen I., Franx M., Kjærgaard P., 1995, MNRAS, 273, 1097

Kennefick J.D., 1996, *Phd Thesis, California Institute of Technology*

Kodama T., Arimoto N., Barger A.J., Aragón-Salamanca A., 1998, A&A, 334, 99

Kodama T., Bell E.F., Bower R.G., 1999, MNRAS, 302, 152

Larson R.B., 1974, MNRAS, 169, 229

Larson R.B., Tinsley B.M., Caldwell N., 1980, ApJ, 237, 692

Ledlow M.J., Owen F.N., 1995, AJ, 109, 853

Lin H., Kirshner R.P., Shectman S.A., Landy S.D., Oemler A., Tucker D.L., Shechter P.L., 1996, ApJ, 464, 60

Newberry M.V., Kirshner R.P., Boroson T.A., 1988, AJ, 335, 629

Oemler A.Jr., Dressler A., Butcher H.R., 1997, ApJ, 474, 561

Pahre M.A., 1998, *Phd Thesis, California Institute of Technology*

Pahre M.A., 1999, submitted to AJ

Picard A., 1991, *Phd Thesis, California Institute of Technology*

Postman M., Huchra J.P., Geller M.J., 1992, ApJ, 384, 404

Rakos K.D., Odell A.P., Schombert J.M., 1997, ApJ, 490, 201

Rakos K.D., Maindl T.I., Schombert J.M., 1996, ApJ, 466, 122

Rakos K.D., Schombert J.M., 1995, ApJ, 439, 47 (RS95)

Rose J.A., Bower R.G., Caldwell N., Ellis R.S., Sharples R.M., Teague P., 1994, AJ, 108, 2054

Slinglend K., Batuski D., Miller C., Haase S., Michaud K., Hill J.M., 1998, ApJS, 115, 1

Smail I., Dressler A., Couch W.J., Ellis R.S., Oemler A.Jr., Butcher H., Sharples R.M., 1997, ApJS, 110, 213

Smail I., Edge A., Ellis R., Blandford R., 1998, MNRAS, 293, 124

Small T., 1996, *Phd Thesis, California Institute of Technology*

Stanford S.A., Eisenhardt P.R., Dickinson M., 1998, ApJ, 492,461

Struble M.F., Rood H.J., 1991, ApJS, 77, 363

Terlevich A.I., Kuntschner H., Bower R.G., Caldwell N., Sharples R.M., 1999, submitted to MNRAS(astro-ph/9907072)

Thuan T.X., Gunn J.E., 1976, PASP, 88, 543

Valdes F., 1982, *Instrumentation in Astronomy IV, S.P.I.E. Proceedings*, Vol. 331, 465

Visvanathan N. & Sandage A., 1977, ApJ, 216, 214

Weir N., 1994, *Phd Thesis, California Institute of Technology*

Worthey G., 1996, review for the *1996 Star Formation Near and Far conference* (astro-ph/9611180)

Yee H.K.C., Gladders M.D., López-Cruz O., 1999, to appear in the proceedings of the OCIW/Pasadena Workshop on Photometric Redshift, held April 1999 (astro-ph/9908001)

This preprint was prepared with the AAS LaTeX macros v4.0.

Table 1. Log of the Observations

ACO	Date	T_{exp}(s)			seeing(")			Lim Mag		
		g	r	i	g	r	i	g	r	i
1134	97, March 08	1800	1200	900	1.60	1.45	1.30	22.7	22.3	21.9
P861C1	97, March 08	1200	900	900	1.79	1.74	1.42	22.5	22.5	21.7
820	97, March 09	900	600	600	1.40	1.44	1.16	22.3	22.1	21.3
827	97, March 09	900	600	600	1.58	1.45	1.48	22.5	22.3	21.7
860	97, March 09	900	600	600	1.47	1.42	1.37	22.3	22.1	21.3
1191	97, March 09	900	600	600	1.58	1.38	1.33	22.5	22.1	21.5
1577	97, March 09	1800	900	900	1.39	1.29	1.27	22.9	22.5	21.9
2066	97, March 09	1800	900	900	1.49	1.26	1.24	22.9	22.5	21.9
810	97, March 10	1800	900	900	1.34	1.41	1.26	22.9	22.3	21.7
1650	97, March 10	900	600	600	1.74	1.68	1.53	22.5	22.1	21.7
1689	97, March 10	900	600	600	1.32	1.20	1.19	22.5	22.3	21.7
2094	97, March 10	1800	900	900	1.21	1.27	1.38	22.7	22.3	21.7
2103	97, March 10	1800	900	900	1.34	1.37	1.32	22.7	22.3	21.7
933	97, March 11	1800	900	900	1.59	1.37	1.48	22.9	22.3	21.7
944	97, March 11	900	600	600	1.41	1.29	1.21	22.5	22.3	21.3
1620	97, March 11	900	600	600	1.37	1.23	1.18	22.5	22.1	21.5
2128	97, March 11	900	600	600	1.27	1.16	1.22	22.3	22.1	21.5
248	97, Nov 23	2700	900	900	1.35	1.46	1.46	23.3	22.7	22.3
508	97, Nov 23	3600	900	900	1.32	1.36	1.43	22.9	23.1	22.7
2700	97, Nov 23	2700	900	900	1.83	1.52	1.52	23.5	22.7	22.1
145	97, Nov 26	1800	900	900	1.67	1.41	1.27	23.1	22.5	21.9
248	97, Nov 26	1800	900	900	1.73	1.46	1.63	23.3	22.3	21.9
324	97, Nov 26	1800	900	900	1.92	1.75	1.67	23.1	22.5	21.5
2700	97, Nov 26	1800	900	900	1.80	1.46	1.37	23.3	22.3	21.9
1200	98, Apr 22	1200	900	900	1.89	1.76	1.55	22.7	22.3	21.9
1260	98, Apr 22	1200	900	900	1.53	1.43	1.54	23.3	22.5	21.7
1238	98, Apr 24	1200	900	900	1.90	1.53	1.31	22.7	22.3	21.7
1373	98, Apr 24	1200	900	900	2.09	1.50	1.40	22.9	22.3	21.7
1525	98, Apr 24	1200	900	900	1.37	1.33	1.31	22.9	22.5	21.9
1882	98, Apr 24	1200	900	900	1.47	1.37	1.39	22.9	22.5	21.9
1993	98, Apr 24	1200	900	900	1.80	1.86	2.15	22.7	22.5	21.7
1399	98, Apr 26	1200	900	900	1.63	1.49	1.43	22.5	22.1	21.5
1938	98, Apr 26	1200	900	900	1.65	1.75	1.60	22.5	22.1	21.7
2051	98, Apr 26	1200	600	600	1.61	1.60	1.46	22.3	21.9	21.3
2053	98, Apr 26	1200	900	900	1.75	1.67	1.53	22.7	22.3	21.5
189	98, Nov 13	2700	900	900	1.74	1.35	1.28	23.5	22.5	21.9
482	98, Nov 13	2700	900	900	1.56	1.70	1.42	23.3	22.7	22.1
2700	98, Nov 13	2700	900	900	1.39	1.11	1.16	23.5	22.5	21.9
352	98, Nov 14	2700	900	900	1.62	1.34	1.47	23.5	22.5	21.9
509	98, Nov 14	2700	900	900	1.24	1.21	1.28	23.3	22.5	21.9
P887C04	98, Nov 14	3600	900	900	1.97	1.56	1.67	23.1	22.3	21.5
261	98, Nov 15	2700	900	900	1.88	1.39	1.88	23.3	22.5	21.9
324	98, Nov 15	2700	900	900	1.43	1.30	1.30	23.3	22.5	21.9

Table 1—Continued

ACO	Date	T_{exp}(s)			seeing(")			Lim Mag		
		g	r	i	g	r	i	g	r	i
776	98, Nov 15	2700	900	900	1.76	1.71	1.49	23.3	22.3	21.7
168	98, Nov 16	2700	900	900	1.58	1.21	1.19	23.5	22.5	21.9
255	98, Nov 16	2700	900	900	1.73	1.49	1.50	23.5	22.5	21.9
P887C05	98, Nov 16	2700	900	900	1.53	1.33	1.47	23.3	22.3	21.7
119	98, Nov 17	2700	900	900	1.69	1.50	1.45	23.5	22.5	21.9
370	98, Nov 17	2700	900	900	1.84	1.83	1.64	23.5	22.7	21.9
477	98, Nov 17	2700	900	900	1.53	1.39	1.31	23.3	22.5	22.1
P887C18	98, Nov 17	2700	900	900	2.02	1.83	1.81	23.3	22.3	21.7

Table 2. Zero points of the magnitude scale

NIGHT	A_g	A_r	A_i
1, 97, March 08	-8.643 ±0.036	-8.388 ±0.011	-8.391 ±0.007
2, 97, March 09	-8.627 ±0.030	-8.382 ±0.016	-8.379 ±0.054
3, 97, March 10	-8.645 ±0.032	-8.392 ±0.008	-8.406 ±0.005
4, 97, March 11	-8.596 ±0.032	-8.366 ±0.009	-8.384 ±0.002
5, 97, Nov 23	-8.296 ±0.026	-7.970 ±0.048	-7.694 ±0.012
6, 97, Nov 26	-8.318 ±0.008	-8.007 ±0.034	-7.706 ±0.007
7, 98, Apr 22	-8.163 ±0.088	-8.079 ±0.018	-8.139 ±0.004
8, 98, Apr 24	-8.141 ±0.073	-8.050 ±0.041	-8.101 ±0.030
9, 98, Apr 26	-8.223 ±0.030	-8.116 ±0.025	-8.180 ±0.074
10, 98, Nov 13	-8.180 ±0.021	-7.966 ±0.029	-8.085 ±0.003
11, 98, Nov 14	-8.185 ±0.025	-7.978 ±0.048	-8.087 ±0.001
12, 98, Nov 15	-8.184 ±0.026	-7.966 ±0.022	-8.098 ±0.019
13, 98, Nov 16	-8.167 ±0.022	-7.944 ±0.035	-8.035 ±0.022
14, 98, Nov 17	-8.183 ±0.022	-7.965 ±0.018	-8.083 ±0.003

Table 3. Characteristics of the Sample

ACO	R.A.(1950)	Dec.(1950)	R	z	Ref.(z)	f_B
119	00 53.8	-01 32	1	0.0440	SR91	-0.098 ± 0.007
145	01 04.2	-02 43	2	0.1909	F93	0.205 ± 0.045
168	01 12.6	-00 1	2	0.0452	SR91	-0.042 ± 0.021
189	01 21.1	+01 23	1	0.0325	SR91	-0.085 ± 0.017
248*	01 42.3	-02 31	1	0.184	pho	0.233 ± 0.047
255	01 44.8	-02 14	1	0.086	pho	0.192 ± 0.041
261	01 48.9	-02 29	1	0.0477	SR91	-0.076 ± 0.019
324*	02 11.2	-01 46	1	0.167	pho	0.108 ± 0.035
352	02 25.6	-02 24	1	0.170	pho	0.159 ± 0.038
370	02 37.3	-01 48	0	0.3750	SR91	0.243 ± 0.054
477	04 09.6	-02 0	1	0.193	pho	0.153 ± 0.031
482	04 14.0	-02 15	1	0.149	pho	0.079 ± 0.027
508	04 43.3	+01 55	2	0.1479	SR91	0.035 ± 0.021
509	04 45.1	+02 12	1	0.0836	SR91	0.024 ± 0.022
776	09 13.7	-00 11	1	0.202	pho	0.163 ± 0.025
810	09 28.2	-01 56	0	0.103	pho	0.004 ± 0.017
820	09 31.3	-02 42	1	0.084	pho	0.112 ± 0.025
827	09 32.1	-02 44	1	0.143	pho	0.213 ± 0.057
860	09 41.0	+02 20	1	0.179	pho	0.207 ± 0.046
933	10 05.1	+00 46	0	0.0951	SR91	-0.047 ± 0.012
944	10 08.6	-01 47	1	0.161	pho	0.108 ± 0.025
1134	10 54.5	-01 52	2	0.108	pho	0.159 ± 0.034
1191	11 08.6	+01 2	2	0.136	pho	0.144 ± 0.025
1200	11 9.8	-02 53	1	0.104	pho	-0.054 ± 0.010
1238	11 20.4	+01 22	1	0.0716	SR91	-0.024 ± 0.017
1260	11 23.8	+02 20	2	0.0492	pho	0.026 ± 0.029
1373	11 42.9	-02 07	2	0.1314	SR91	0.136 ± 0.031
1399	11 48.6	-02 49	2	0.0913	SR91	0.185 ± 0.041
1525	12 19.5	-00 52	3	0.2590	SR91	0.121 ± 0.029
1577	12 35.3	-00 0	1	0.133	pho	0.101 ± 0.028
1620	12 47.2	-01 19	0	0.0825	LO95	0.035 ± 0.022
1650	12 56.2	-01 29	2	0.0845	SR91	-0.011 ± 0.012
1689	13 09.0	-01 6	4	0.1832	SR91	0.093 ± 0.019
1882	14 12.1	-00 06	3	0.110	pho	0.140 ± 0.026
1938	14 35.2	-00 03	1	0.163	pho	0.086 ± 0.027
1993	14 53.4	+02 03	1	0.245	pho	0.606 ± 0.141
2026	15 06.0	-00 05	1	0.0874	SR91	-0.120 ± 0.002
2051	15 14.2	-00 46	2	0.205	pho	0.233 ± 0.054
2053	15 14.7	-00 30	1	0.1127	SR91	0.191 ± 0.040
2066	15 21.4	+01 13	2	0.144	pho	0.087 ± 0.020
2094	15 34.0	-01 52	1	0.1445	S98	0.245 ± 0.046
2103	15 37.3	-02 0	0	0.101	pho	0.088 ± 0.041
2128	15 46.3	-02 54	0	0.1019	P92	0.008 ± 0.024
2700**	00 01.3	+01 47	1	0.0978	SR91	0.145 ± 0.043

Table 3—Continued

ACO	R.A.(1950)	Dec.(1950)	R	z	Ref.(z)	f_B
P861C01	00 23.5	+01 28	···	0.065	pho	0.017 ± 0.025
P887C04	06 39.1	+02 34	···	0.150	pho	0.077 ± 0.030
P887C05	08 34.3	+01 42	···	0.229	pho	0.131 ± 0.033
P887C18	09 18.2	+01 09	···	0.126	pho	0.062 ± 0.029

*mean of two observations

**mean of three observations

SR91 - Struble & Rood 1991

F93 - Fetisova et al. 1993

LO95 - Ledlow & Owen 1995

S98 - Slinglend et al. 1998

P92 - Postman et al. 1992

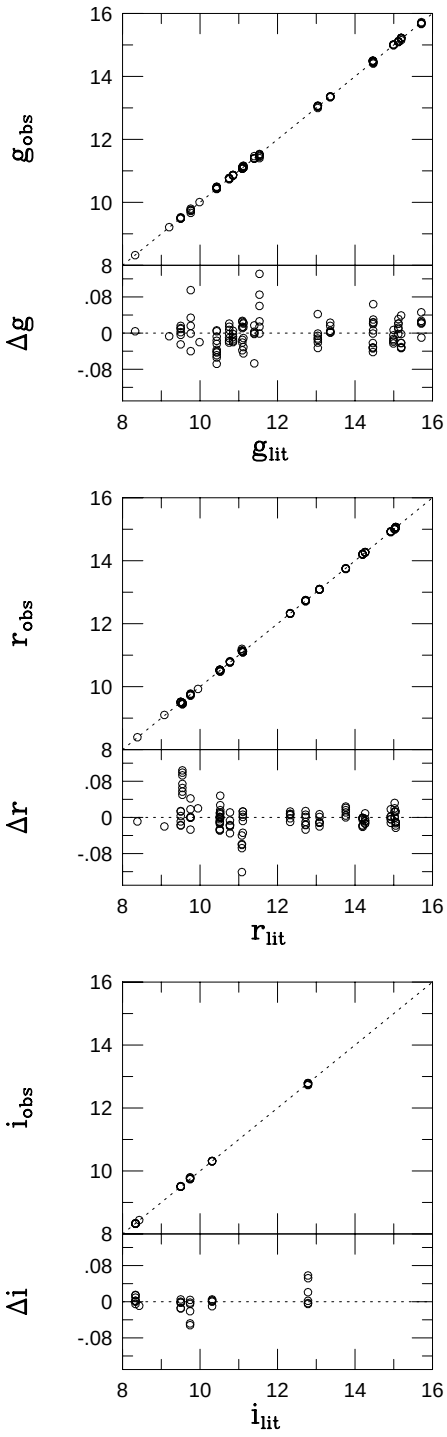

Fig. 1.— Comparison between the magnitudes of standard stars published by Thuan & Gunn (1976) and our calibrated measurements.

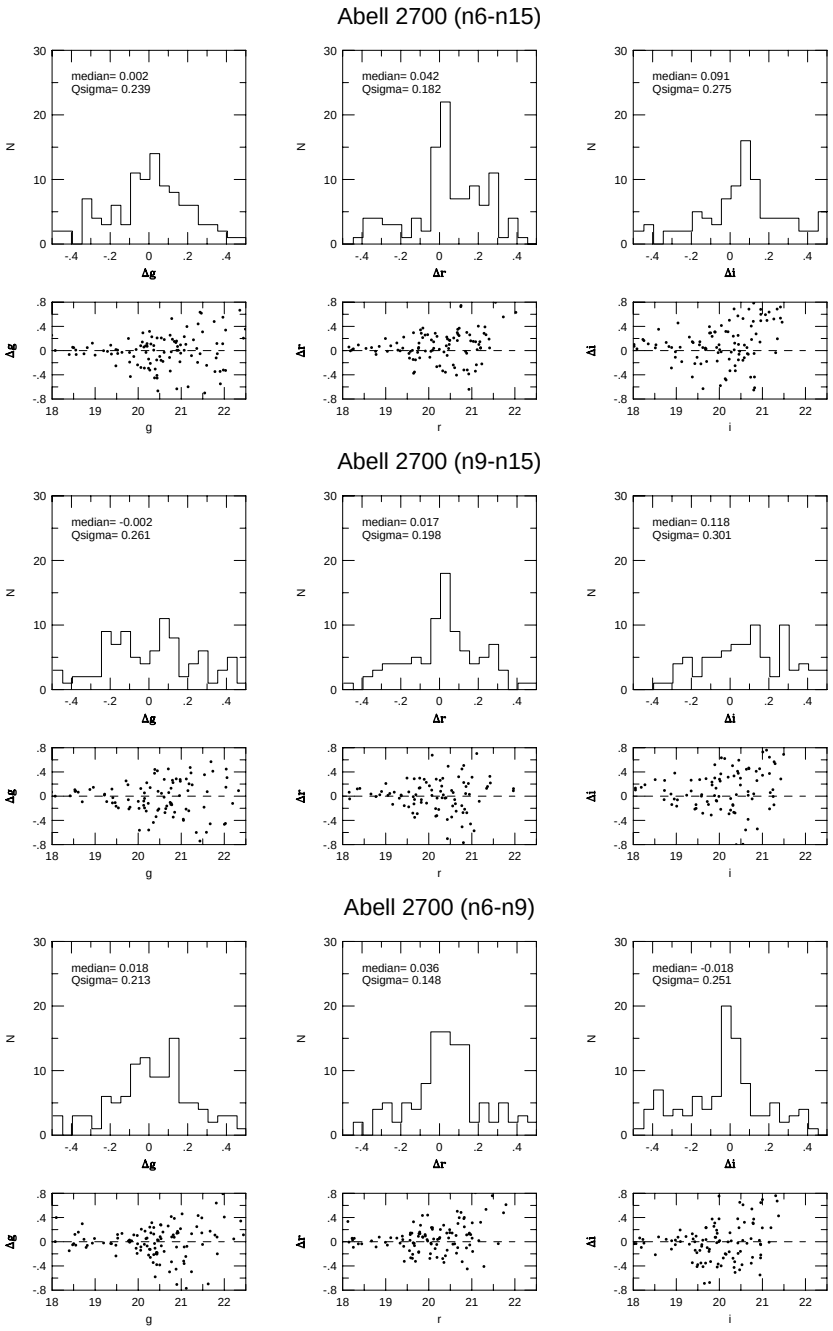

Fig. 2.— Histogram of the magnitude residuals and its correlation with apparent magnitude for Abell 2700. The figure show comparisons between measurements obtained in three different nights.

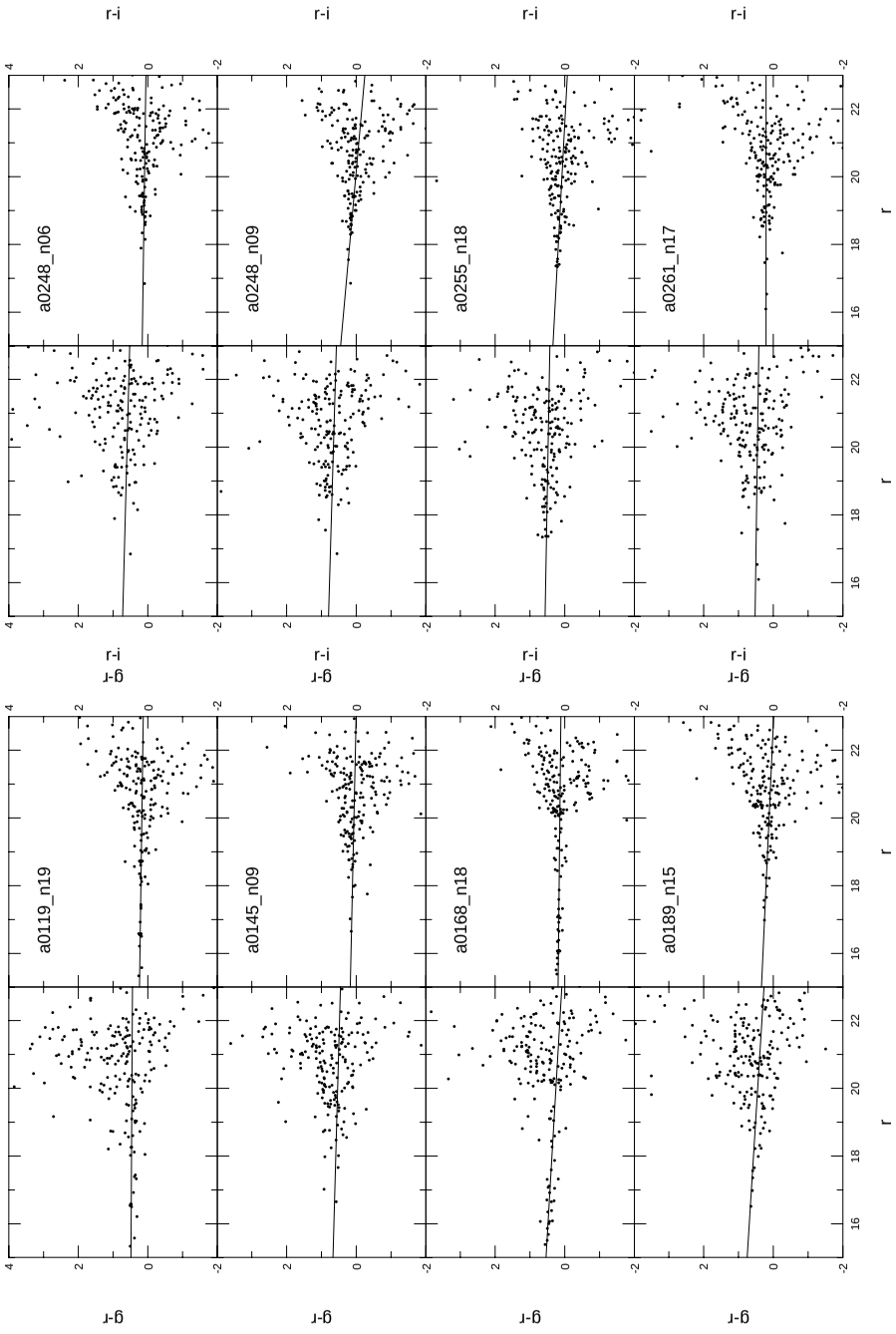

Fig. 3.— $g - r \times r$, and $r - i \times r$ color-magnitude diagrams for the cluster sample. The solid lines indicates the fitting of a linear relation which represents the locus of early-type galaxies.

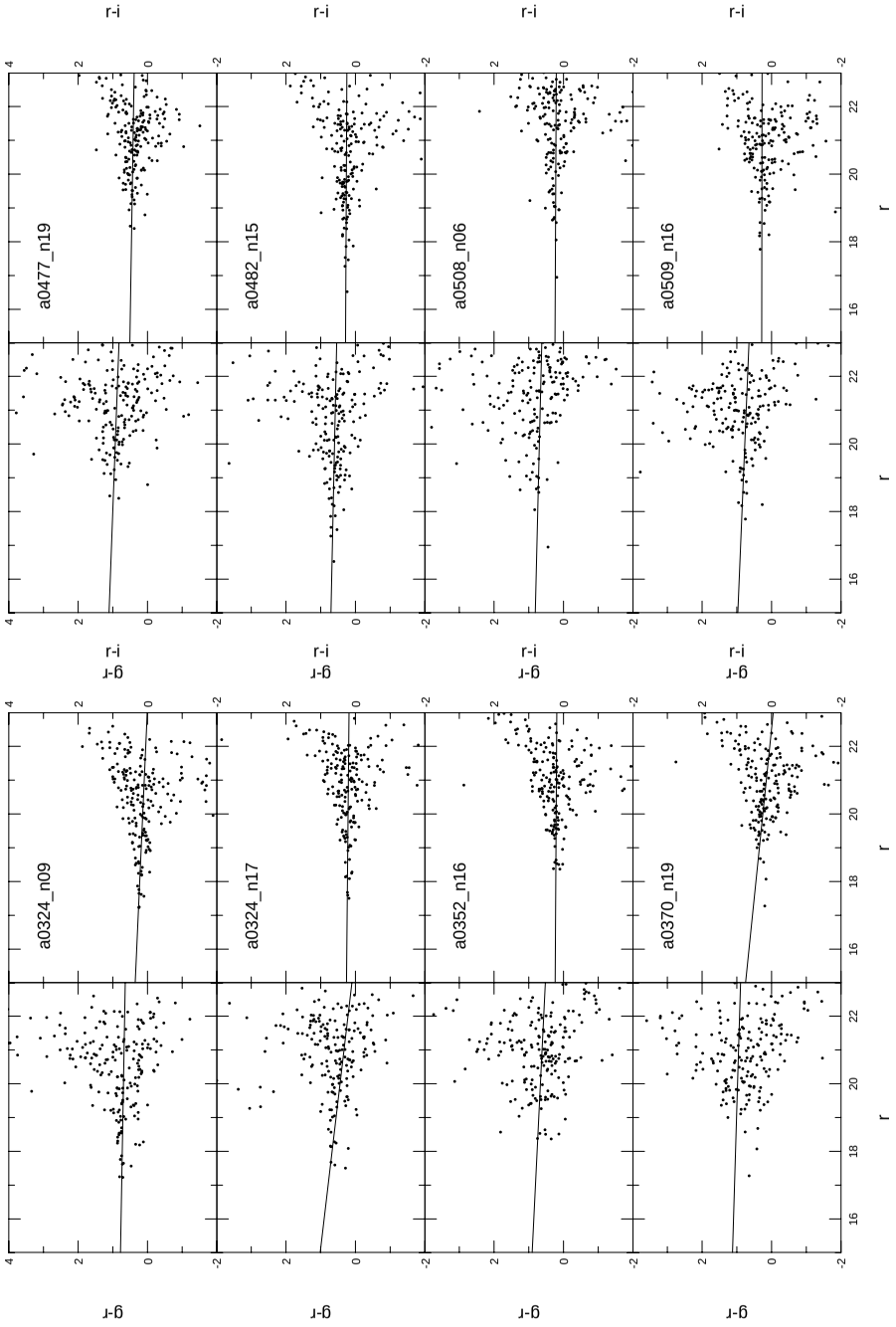

Fig. 3.— Continued.

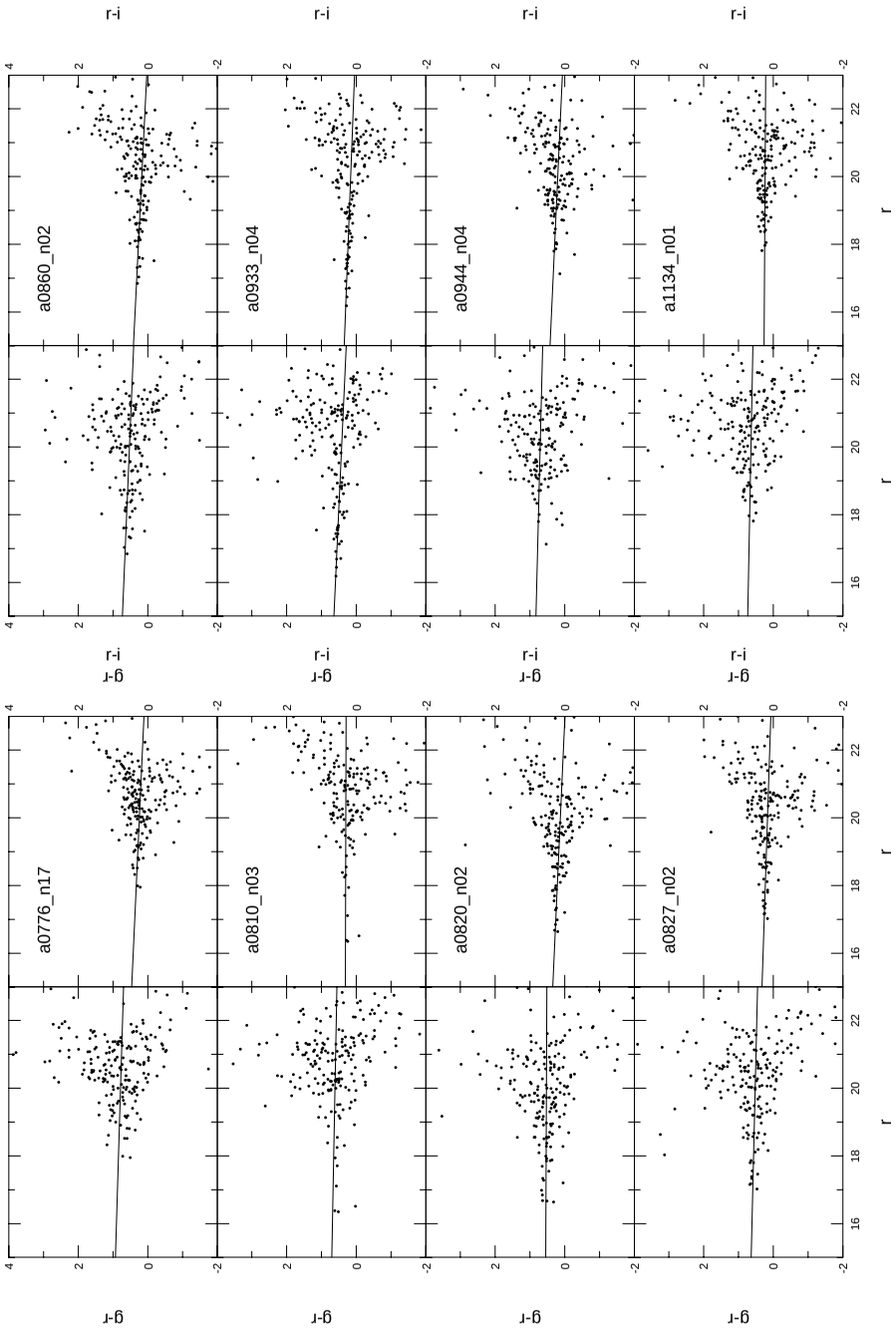

Fig. 3.— Continued.

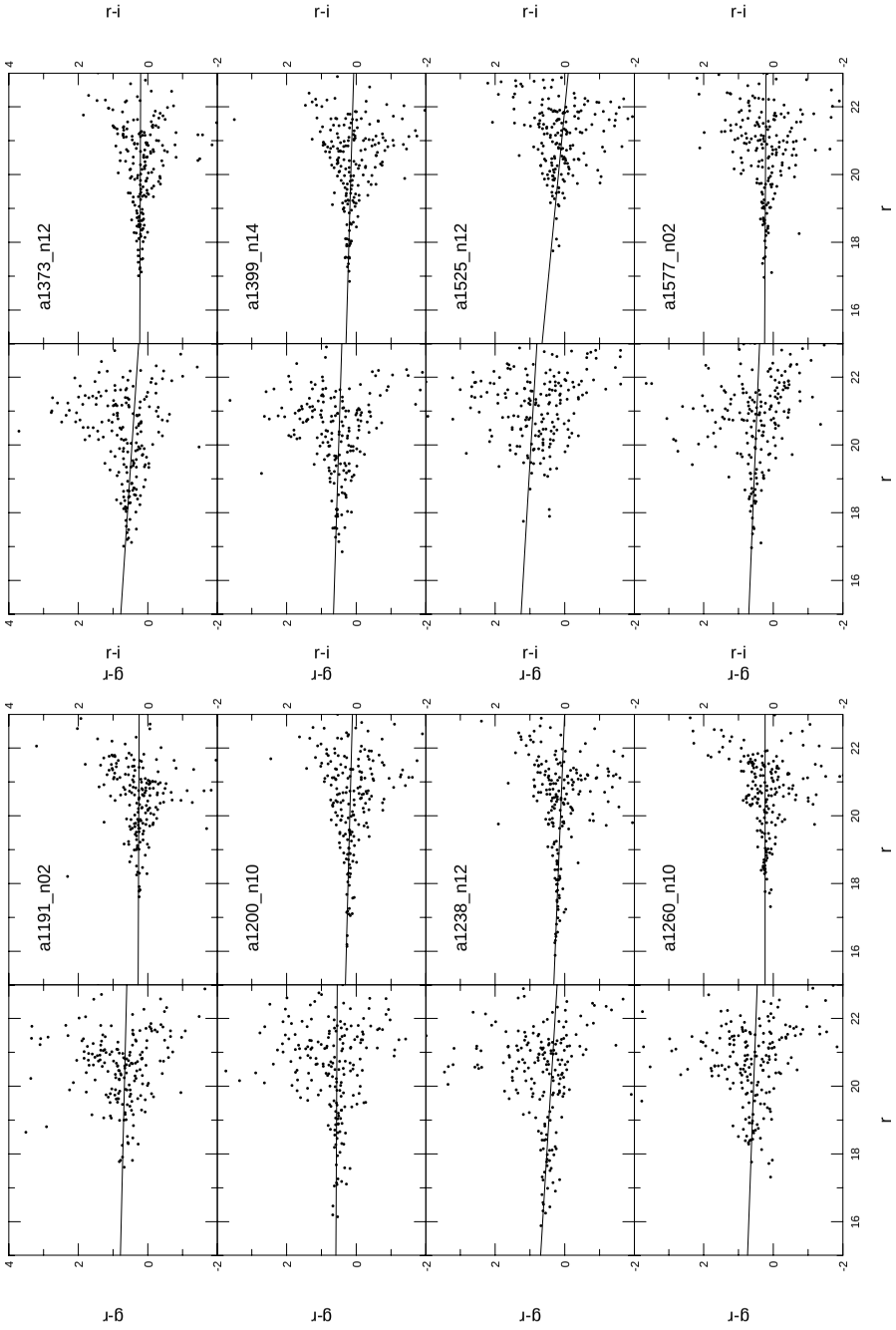

Fig. 3.— Continued.

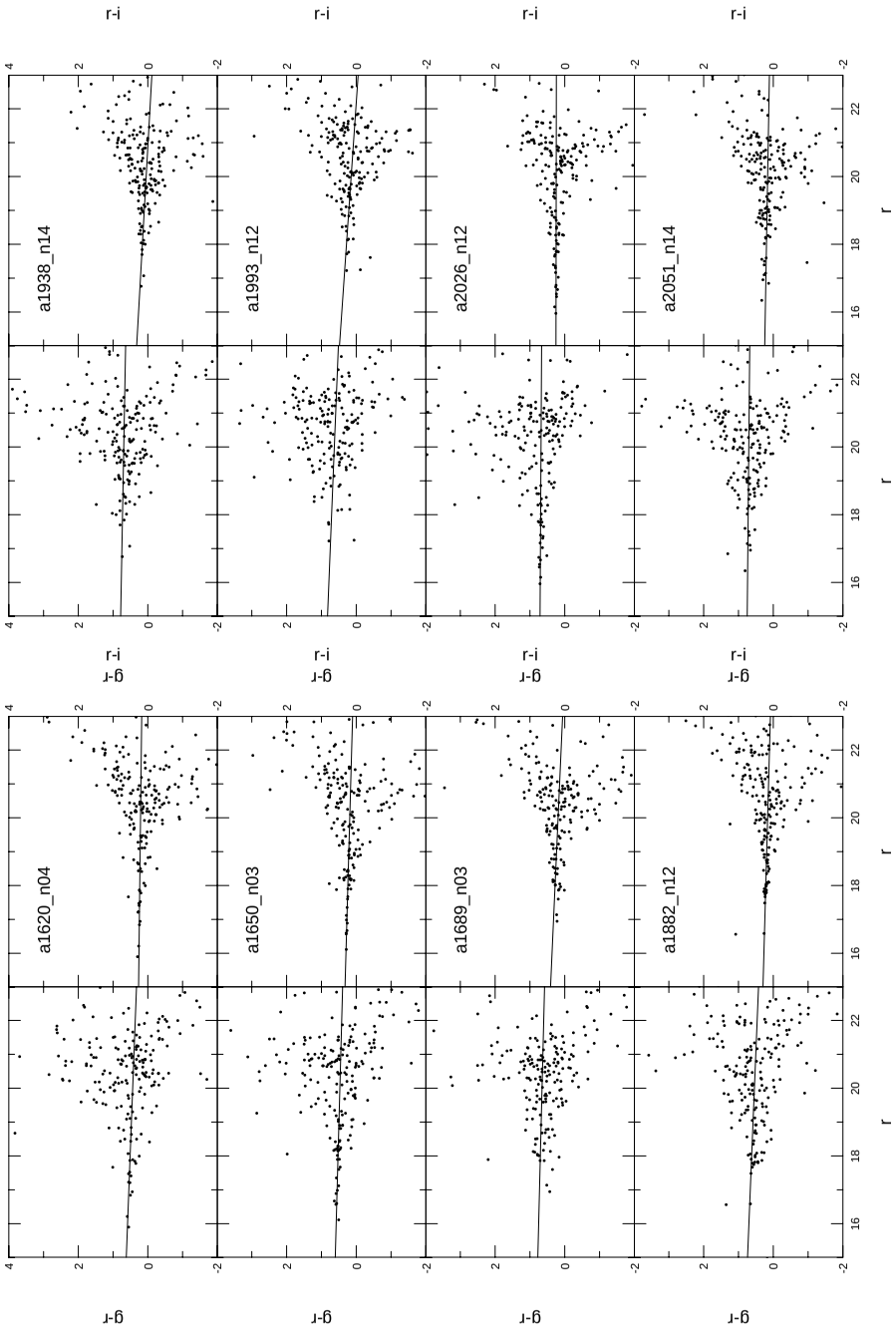

Fig. 3.— Continued.

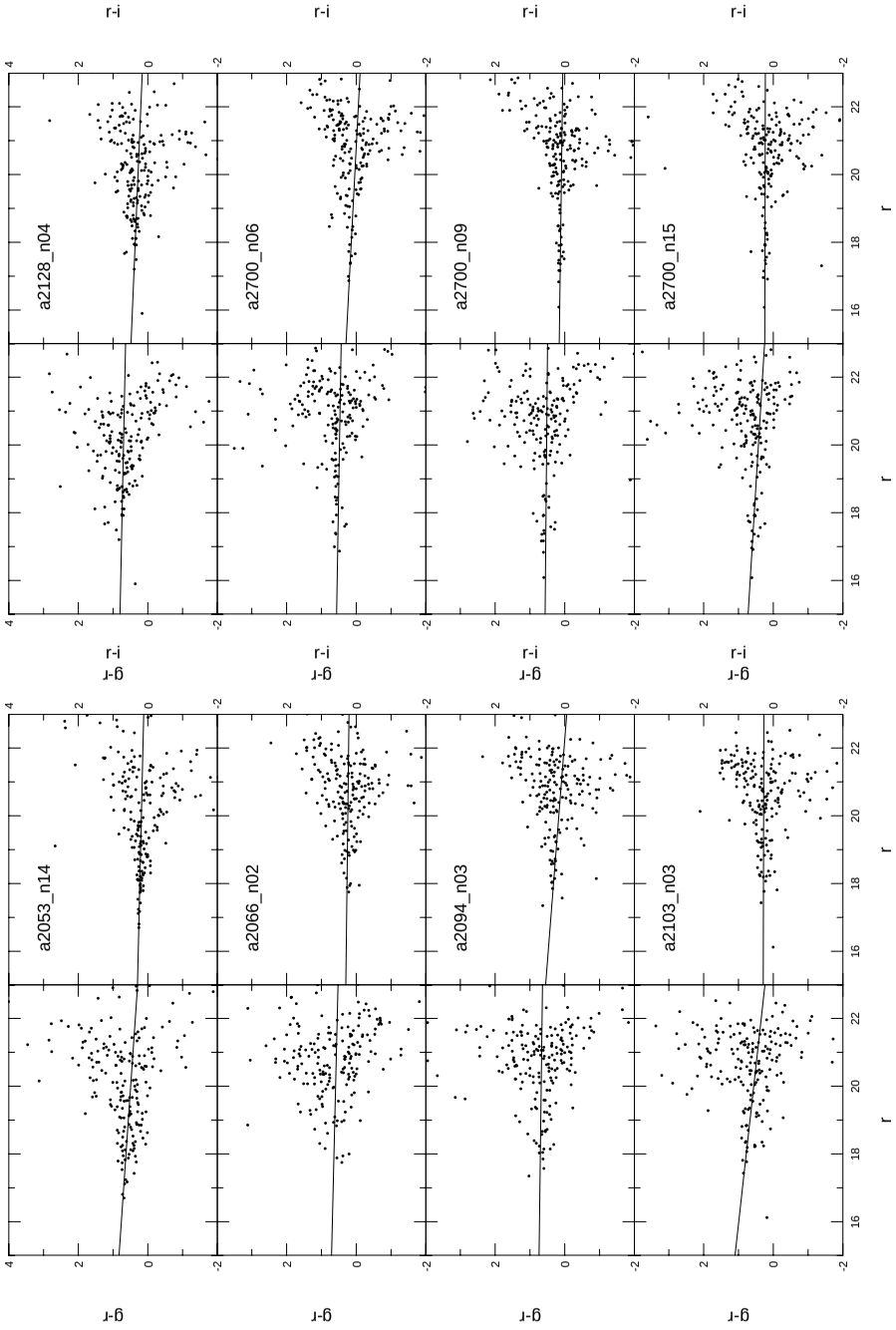

Fig. 3.— Continued.

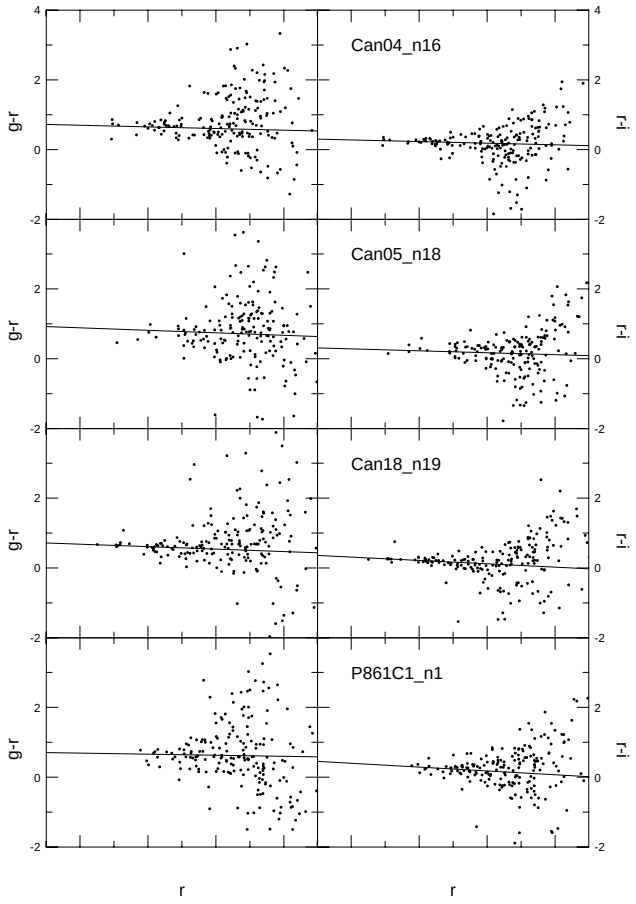

Fig. 3.— Continued.

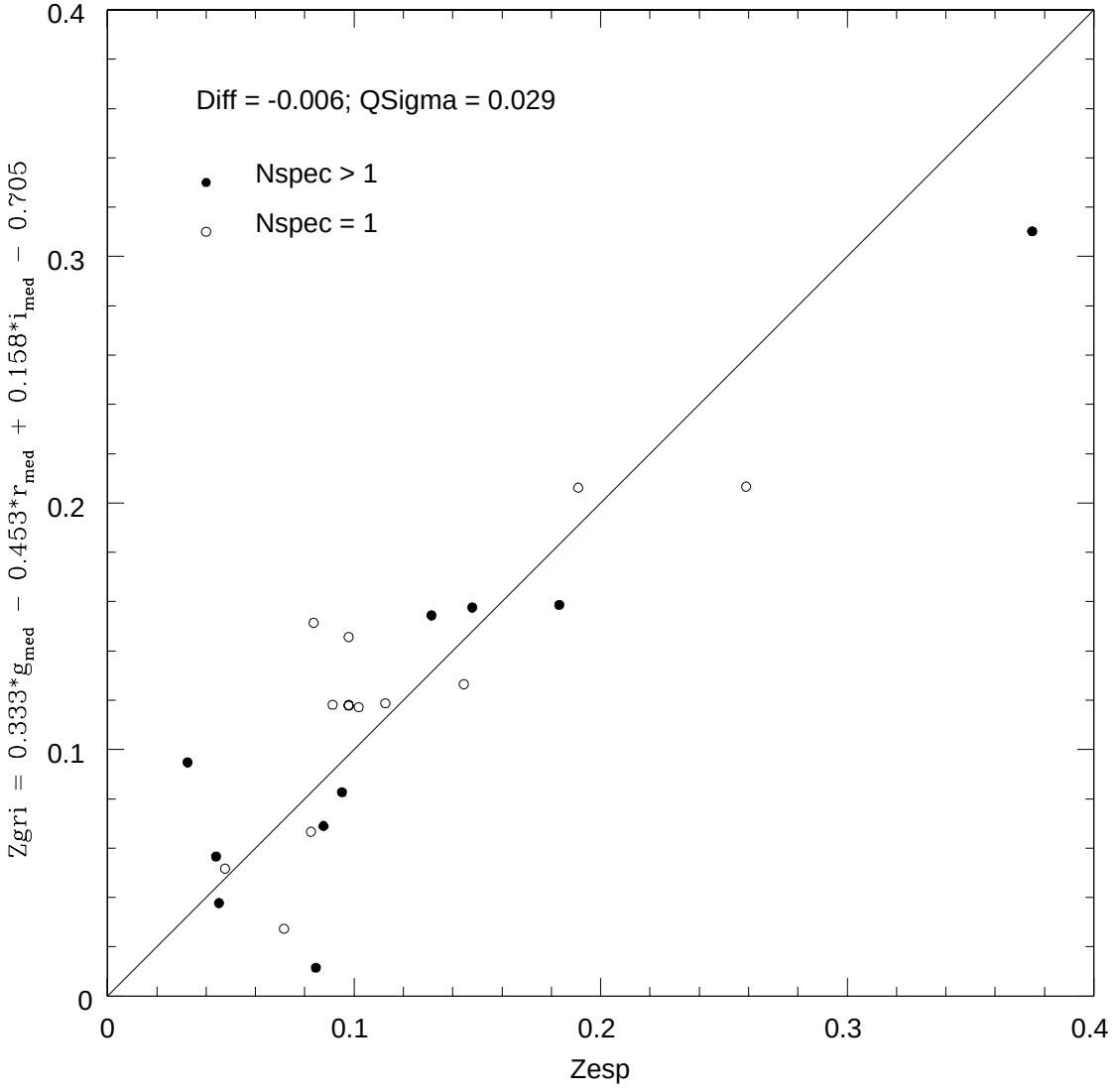

Fig. 4.— Comparison between spectroscopic and photometric redshift.

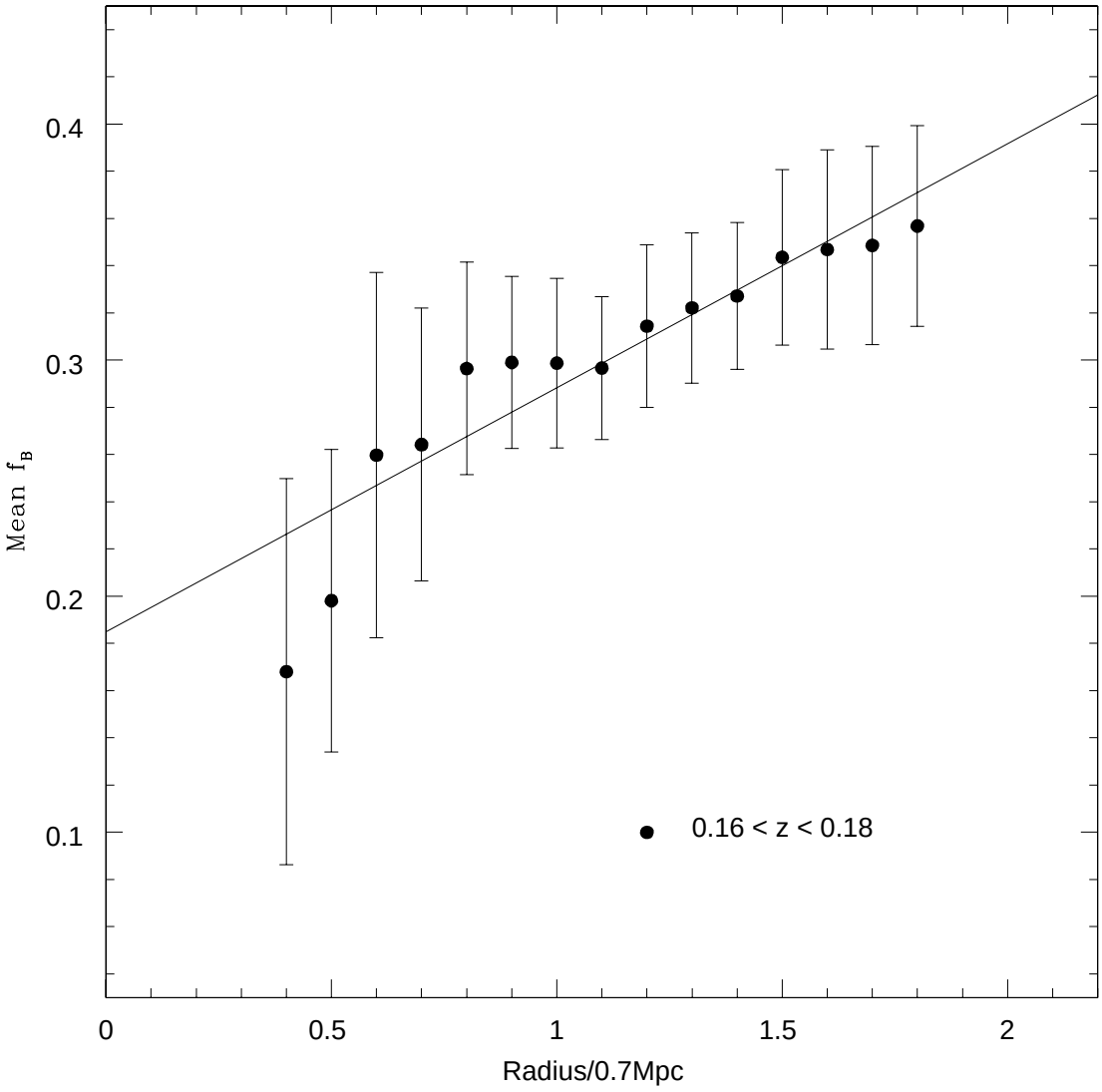

Fig. 5.— Dependence of the fraction of blue galaxies with the physical region of a cluster.

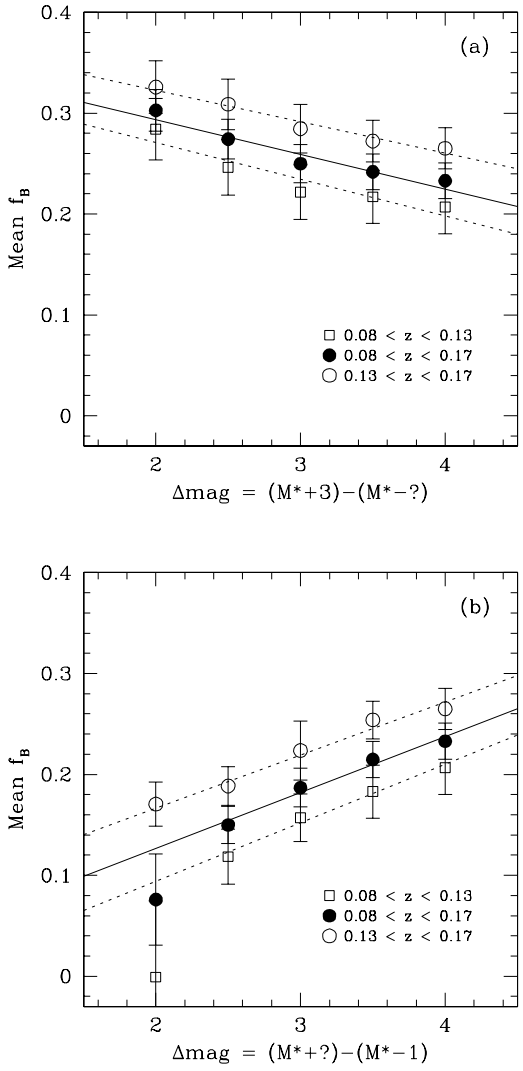

Fig. 6.— Dependence of the fraction of blue galaxies with the interval of the luminosity function used to compute it. The plot shows the effect of: (a) loosing bright objects and observing only an interval $\Delta_{mag} = (M^*+3)-(M^*-?)$; (b) loosing the faintest objects and observing only an interval $\Delta_{mag} = (M^*+?) - (M^* - 1)$.

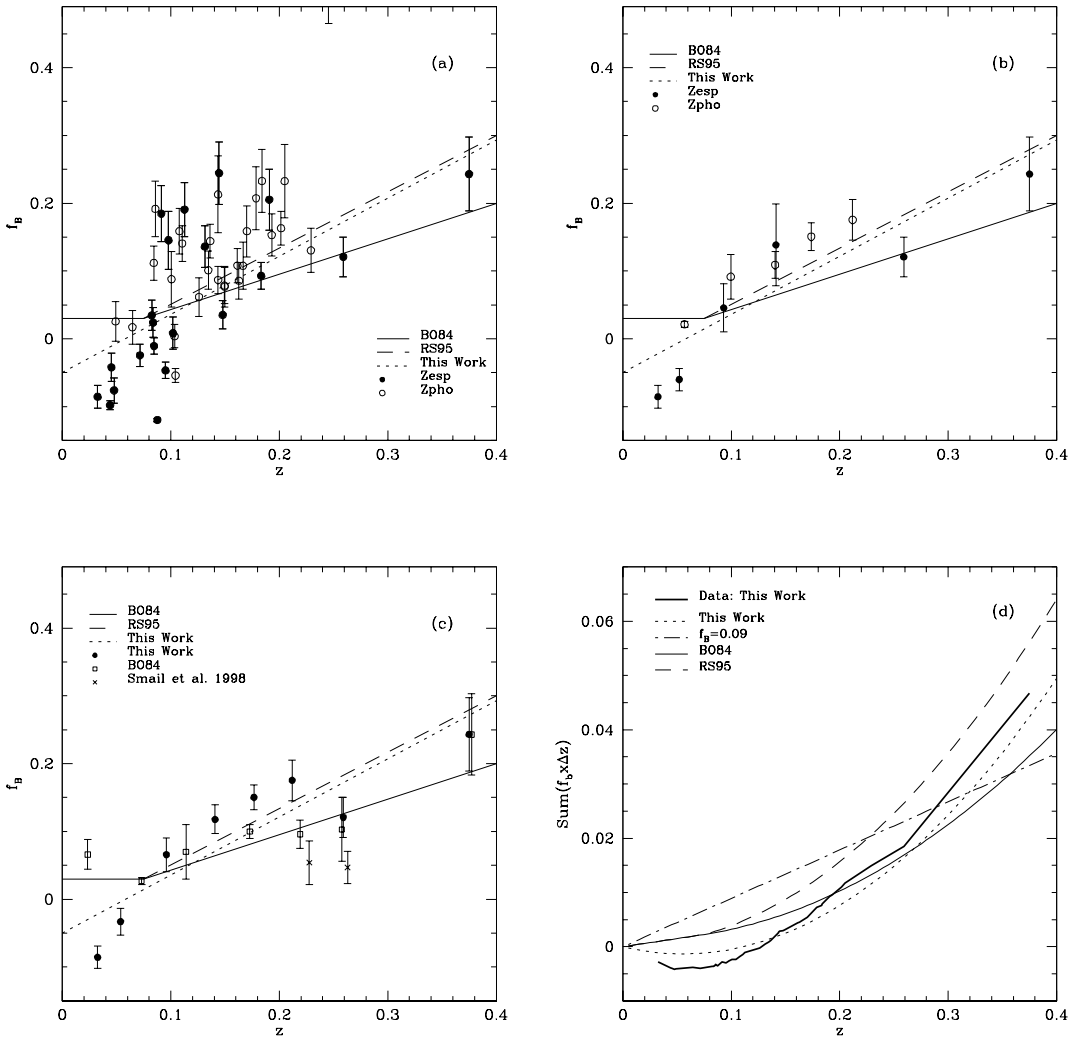

Fig. 7.— (a) Fraction of blue galaxies, with $M^* - 1 \leq M_r \leq M^* + 3$, detected in the central region ($R \leq 0.70$Mpc) of the clusters in our sample; (b) Comparison between mean f_B values (for intervals of 0.4 in redshift) of clusters with spectroscopic and photometric redshifts; (c) Mean f_B for BO84, Smail et al. (1998), and for our sample of clusters with spectroscopic redshifts; (d) accumulated product of $f_B \times \Delta_z$ for the data, BO84 and RS95 relations, and for a constant f_B of 0.10.

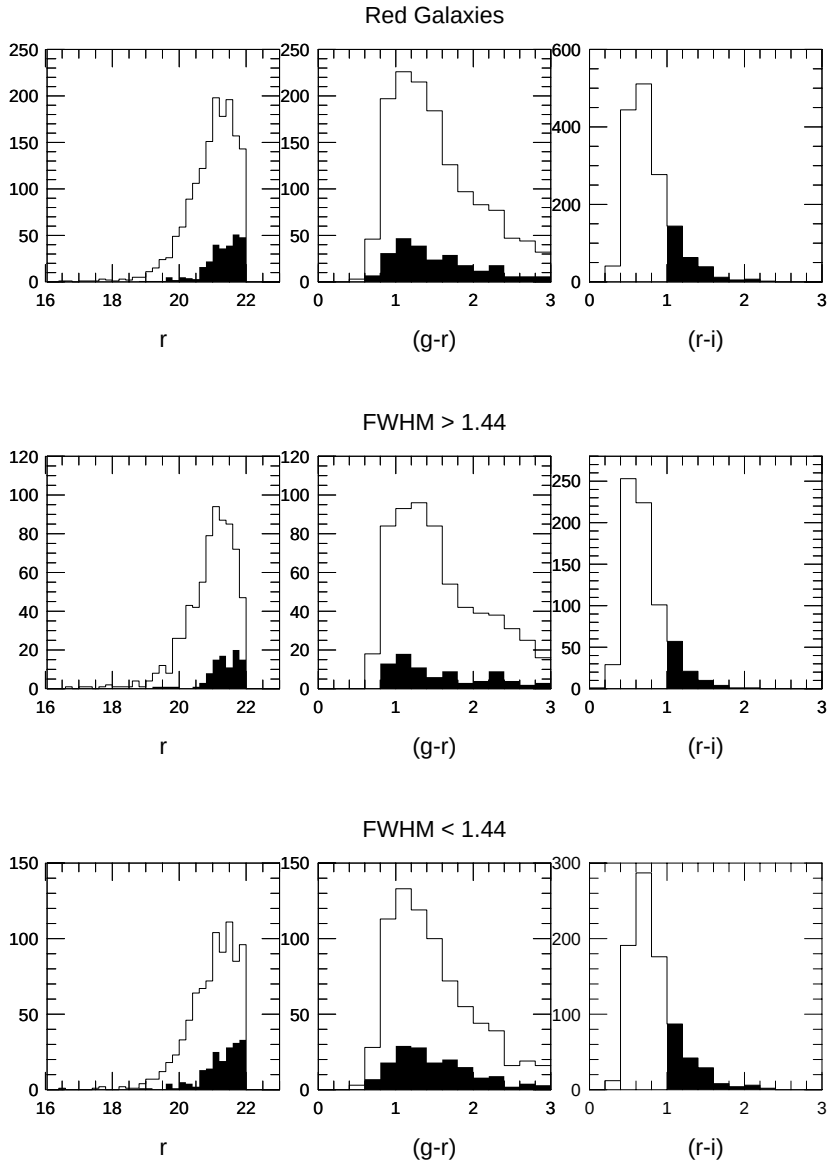

Fig. 8.— Histograms of m_r, $g-r$, and $r-i$ for the red galaxies, and for the anomalously red galaxied (filled histogram). The upper panels show the histograms for all red galaxies detected in our sample. The central panels presents the histograms for the "bad" seeing images ($FWHM > 1.44$), and the "good" seeing images ($FWHM < 1.44$) are represented in the lower panels.